Theses and Dissertations   1. Thesis and Dissertation Collection, all items

2020

THE EFFECTS OF WAVE-INDUCED LOADS ON ROV PERFORMANCE WHILE OPERATING AT NEAR-SURFACE DEPTHS

Marks, Johnathan D.

Monterey, CA; Naval Postgraduate School

http://hdl.handle.net/10945/65400

NAVAL POSTGRADUATE SCHOOL

MONTEREY, CALIFORNIA

THESIS

THE EFFECTS OF WAVE-INDUCED LOADS ON ROV PERFORMANCE WHILE OPERATING AT NEAR-SURFACE DEPTHS

by

Johnathan D. Marks

June 2020

Thesis Advisor: Joseph Klamo
Second Reader: Fotis A. Papoulias

Approved for public release. Distribution is unlimited.

THIS PAGE INTENTIONALLY LEFT BLANK

REPORT DOCUMENTATION PAGE		*Form Approved OMB No. 0704-0188*

Public reporting burden for this collection of information is estimated to average 1 hour per response, including the time for reviewing instruction, searching existing data sources, gathering and maintaining the data needed, and completing and reviewing the collection of information. Send comments regarding this burden estimate or any other aspect of this collection of information, including suggestions for reducing this burden, to Washington headquarters Services, Directorate for Information Operations and Reports, 1215 Jefferson Davis Highway, Suite 1204, Arlington, VA 22202-4302, and to the Office of Management and Budget, Paperwork Reduction Project (0704-0188) Washington, DC 20503.

1. AGENCY USE ONLY (*Leave blank*)	2. REPORT DATE June 2020	3. REPORT TYPE AND DATES COVERED Master's thesis
4. TITLE AND SUBTITLE THE EFFECTS OF WAVE-INDUCED LOADS ON ROV PERFORMANCE WHILE OPERATING AT NEAR-SURFACE DEPTHS		**5. FUNDING NUMBERS**
6. AUTHOR(S) Johnathan D. Marks		
7. PERFORMING ORGANIZATION NAME(S) AND ADDRESS(ES) Naval Postgraduate School Monterey, CA 93943-5000		**8. PERFORMING ORGANIZATION REPORT NUMBER**
9. SPONSORING / MONITORING AGENCY NAME(S) AND ADDRESS(ES) N/A		**10. SPONSORING / MONITORING AGENCY REPORT NUMBER**
11. SUPPLEMENTARY NOTES The views expressed in this thesis are those of the author and do not reflect the official policy or position of the Department of Defense or the U.S. Government.		
12a. DISTRIBUTION / AVAILABILITY STATEMENT Approved for public release. Distribution is unlimited.		**12b. DISTRIBUTION CODE** A

13. ABSTRACT (maximum 200 words)

The objective of this research was to quantify the undesired pitch and heave motions caused by wave-induced loads on a remotely operated vehicle (ROV) operating near the surface. Accomplishing this objective will help to inform system design requirements necessary to ensure desired performance during operations. An experimental study was conducted utilizing a towing tank with wave-making capability and a commercially available ROV. The ROV was tested in the tank at near-surface depths using both single-component and two-component waves for zero speed and forward speed conditions. Pitch, depth, and thruster data were collected from the ROV and compared against control runs to determine the effect of the wave-induced loads on the ability of the ROV to control pitch and maintain depth. For pitch, the results showed that the response had components from linear loads, nonlinear loads, and natural system frequencies. Linear loads resulted in a pitch response that increased with wavelength and ROV speed. Low-frequency nonlinear loads resulted in a measurable pitch response at the wave component frequency differences used. Natural system frequencies resulted in a pitch response at frequencies specific to the ROV, and this response increased with speed. For depth, little response was seen due to the control authority of the ROV; however, the vertical thruster response showed that wave-induced loads have the potential to affect depth if sufficient control authority is not present.

14. SUBJECT TERMS ROV, remotely operated vehicle, near-surface, wave-induced loads			**15. NUMBER OF PAGES** 67
			16. PRICE CODE
17. SECURITY CLASSIFICATION OF REPORT Unclassified	**18. SECURITY CLASSIFICATION OF THIS PAGE** Unclassified	**19. SECURITY CLASSIFICATION OF ABSTRACT** Unclassified	**20. LIMITATION OF ABSTRACT** UU

NSN 7540-01-280-5500

Standard Form 298 (Rev. 2-89)
Prescribed by ANSI Std. 239-18

THIS PAGE INTENTIONALLY LEFT BLANK

THE EFFECTS OF WAVE-INDUCED LOADS ON ROV PERFORMANCE WHILE OPERATING AT NEAR-SURFACE DEPTHS

Johnathan D. Marks
Lieutenant, United States Navy
BS, Texas A & M University, 2013

Submitted in partial fulfillment of the
requirements for the degree of

MASTER OF SCIENCE IN SYSTEMS ENGINEERING

from the

NAVAL POSTGRADUATE SCHOOL
June 2020

Approved by: Joseph Klamo
Advisor

Fotis A. Papoulias
Second Reader

Ronald E. Giachetti
Chair, Department of Systems Engineering

THIS PAGE INTENTIONALLY LEFT BLANK

ABSTRACT

The objective of this research was to quantify the undesired pitch and heave motions caused by wave-induced loads on a remotely operated vehicle (ROV) operating near the surface. Accomplishing this objective will help to inform system design requirements necessary to ensure desired performance during operations. An experimental study was conducted utilizing a towing tank with wave-making capability and a commercially available ROV. The ROV was tested in the tank at near-surface depths using both single-component and two-component waves for zero speed and forward speed conditions. Pitch, depth, and thruster data were collected from the ROV and compared against control runs to determine the effect of the wave-induced loads on the ability of the ROV to control pitch and maintain depth. For pitch, the results showed that the response had components from linear loads, nonlinear loads, and natural system frequencies. Linear loads resulted in a pitch response that increased with wavelength and ROV speed. Low-frequency nonlinear loads resulted in a measurable pitch response at the wave component frequency differences used. Natural system frequencies resulted in a pitch response at frequencies specific to the ROV, and this response increased with speed. For depth, little response was seen due to the control authority of the ROV; however, the vertical thruster response showed that wave-induced loads have the potential to affect depth if sufficient control authority is not present.

THIS PAGE INTENTIONALLY LEFT BLANK

Table of Contents

List of Figures

THIS PAGE INTENTIONALLY LEFT BLANK

List of Tables

THIS PAGE INTENTIONALLY LEFT BLANK

List of Acronyms and Abbreviations

AUV   autonomous underwater vehicle

MCM   mine countermeasures

NPS   Naval Postgraduate School

PSD   power spectral density

RAO   response amplitude operator

ROV   remotely operated vehicle

RPM   revolutions per minute

UUV   unmanned underwater vehicle

THIS PAGE INTENTIONALLY LEFT BLANK

Executive Summary

The objective of this research is to quantify the undesired pitch and heave motions caused by wave-induced loads on a remotely operated vehicle (ROV) operating near the surface. These motions were explored for an ROV attempting to hold speed, heading, and depth. Accomplishing this objective will help to inform system design requirements necessary to ensure desired performance during operations. It will also help to inform ROV capabilities and limitations, such as minimum operating depth and maximum sea state, that can be used in the mission-planning process.

To achieve the desired objective, an experimental study was conducted to test the performance of an ROV operating at near-surface depths under a variety of conditions. For the purposes of this study, a near-surface depth was defined as a depth close enough to the surface to experience the effects of waves. The maximum depth at which surface wave effects can still be experienced is approximated as a depth no greater than one-half the wavelength.

The ROV tested was a Blue Robotics BlueROV2 in a six-thruster vectored configuration with two vertical thrusters and four horizontal thrusters. Testing was conducted in a towing tank with wave making capability located at the Naval Postgraduate School. The tank was used to generate both single-component and two-component waves which were characterized using a nondimensional wavelength parameter defined as the ratio of wavelength and ROV length. Additionally, a nondimensional depth parameter was used and defined as the ratio of ROV centerline depth and ROV equivalent diameter. Equivalent diameter was defined as the diameter of a circle with an equivalent cross-sectional area to the ROV. The ROV was tested using a single nondimensional depth and various nondimensional wavelengths at both zero speed and forward speeds while operating in a depth hold mode. Pitch, depth, and thruster data from the ROV were collected and used to make a comparison between calm water and wave environments and to identify any potential changes in performance due to wave-induced loads.

The effects of surface waves on the ROV resulted in unwanted pitch responses stemming from linear loads, nonlinear loads at wave frequency differences for two-component waves, and the natural frequencies of the system. For linear loads, it was shown that the amplitude

of the pitch response increased with wavelength, decreased with speed, and scaled linearly with wave amplitude. It was also shown that the pitch response due to linear loads for a single-component wave could be superimposed to generate the response due to linear loads for a two-component wave and potentially for n number of wave components. The behavior of the pitch response due to the low frequency nonlinear loads that occur at wave frequency differences could not be determined since the frequency difference range examined was small. The pitch response at the natural system frequencies was shown to be independent of wavelength and wave amplitude but dependent on speed as the response increased with increased speed.

Due to the ability of the ROV to maintain depth while in the depth hold mode, the depth response resulting from surface wave effects was minimal. Using the depth hold mode, the ROV had sufficient vertical control authority and response time to minimize the response from wave-induced loads. The existence of these loads in the vertical direction that the ROV was able to overcome was confirmed by examining the thruster response. The thruster response due to linear loads demonstrated similar behavior to the pitch response in its dependence on wavelength. For an unmanned underwater vehicle which lacks sufficient control authority for depth, it is expected that the depth response would follow a similar behavior and dependence on wavelength as pitch did for the ROV. The depth and thruster responses at the natural system frequencies also showed a similar behavior to the pitch response which was independent of wavelength and wave amplitude but dependent on speed. However, this behavior is only applicable to the BlueROV2 as the frequencies are inherent to the ROV.

The results of this study have the potential to enable the development of a dynamic model of the vehicle response which could be used for design optimization as well as improved control systems and autonomous operations. However, this study accounted for a select number of wave encounter frequencies, a single wave heading and depth, and had limited control over speed. To better understand the response behavior, additional data would need to be collected for an increased number of frequencies, depths, speeds, and wave headings. Additionally, further multi-component wave testing could also help determine the response behavior due to nonlinear loads from the frequency difference between underlying component waves in a complex seaway.

Acknowledgments

I would like to thank my thesis advisor, Dr. Klamo, for his guidance and optimism throughout the process of completing this thesis, and my second reader, Dr. Papoulias, for his support not only with this thesis but with my other academic ventures as well. I would also like to thank Albert Jordan and Rushen Dal from the Systems Engineering Department for their technical advice and support.

THIS PAGE INTENTIONALLY LEFT BLANK

CHAPTER 1:
Introduction

1.1 Problem Introduction

As unmanned systems have progressed in technological maturity, they have grown to play a key role in accomplishing missions throughout the Department of Defense. For the Navy in particular, unmanned underwater vehicles (UUVs) have been used to accomplish a variety of missions related to undersea warfare such as anti-submarine warfare; anti-surface warfare; intelligence, surveillance, and reconnaissance; naval special warfare; and mine countermeasures (MCM) [1]. Two types of UUVs in use by the Navy are autonomous underwater vehicles (AUVs), which operate without a man-in-the-loop, and remotely operated vehicles (ROVs), which operate with a man-in-the-loop. A prime example of these two types of UUVs are the systems used by expeditionary MCM companies. These systems are the Mk 18 Mod 1 and Mod 2, based on the Hydroid REMUS 100 and REMUS 600 AUVs, and the Teledyne SeaBotix ROV. Figure 1.1 and Figure 1.2 show the Mk 18 Mod 2 AUV and the Seabotix ROV in use, respectively.

Figure 1.1. Sailors launch a Mk 18 Mod 2 AUV from a small boat. Source: [2].

With the number and complexity of missions performed by UUVs increasing, so to does the importance of understanding the factors that affect their performance during a mission. UUVs typically operate in deeper waters within the open ocean. However, the recent shift in focus by the Navy to increase operations within the littorals requires UUVs to operate in shallower waters and closer to the surface. Furthermore, even when operating in the open ocean, UUVs are still required to operate at or near the surface when being launched or retrieved, acquiring fixes for navigation, or relaying communications. One consideration for the performance of UUVs operating at near-surface depths is the increased interaction with surface waves.

Figure 1.2. A Sailor launches a SeaBotix ROV from a small boat. Source: [3].

Waves propagating along the surface of the ocean impart a circular motion on the water particles they pass through. The radius of this circular motion and the velocity of the water particles are largest at the surface and decrease with depth. Therefore, UUVs operating near the surface experience an increase in wave motion and, subsequently, an increase in wave-induced loads. Since UUVs are designed to typically operate in deeper waters, they may not be capable of compensating for the increase in loads experienced near the surface. This could result in unintended behavior, such as surface breaching, or an inability to maintain attitude using control surfaces. Consequences of this unintended behavior could include a decrease in mission performance or even a loss of the UUV.

1.2   Research Objective

The objective of this research is to quantify the undesired pitch and heave motions caused by wave-induced loads on an ROV operating near the surface. These motions will be explored for an ROV attempting to hold speed, heading, and depth. Accomplishing this objective will help to inform system design requirements necessary to ensure desired performance during operations. It will also help to inform ROV capabilities and limitations, such as minimum operating depth and maximum sea state, that can be used in the mission-planning process.

1.3   Research Methodology

An experimental study was conducted to test the performance of an ROV operating at near-surface depths under a variety of conditions. For the purposes of this study, a near-surface depth was defined as a depth close enough to the surface to experience the effects of waves. The maximum depth at which surface wave effects can still be experienced is approximated as a depth no greater than one-half the wavelength.

Testing was conducted in a towing tank with wave making capability. The tank was used to generate both single-component and two-component waves which were characterized using a nondimensional wavelength parameter defined as the ratio of wavelength and ROV length. Additionally, a nondimensional depth parameter was used and defined as the ratio of ROV centerline depth and ROV equivalent diameter. Equivalent diameter was defined as the diameter of a circle with an equivalent cross-sectional area to the ROV. The ROV was tested using a single nondimensional depth and various nondimensional wavelengths at both zero speed and forward speed. Pitch, depth, and thruster data from the ROV were collected and used to make a comparison between calm water and wave environments and to identify any potential changes in performance due to wave-induced loads.

1.4   Thesis Organization

The remainder of this thesis is organized as follows. Chapter 2 presents previous research conducted. Chapter 3 describes the experimental setup and procedure. Chapter 4 details data collection and reduction. Chapter 5 provides an analysis of the results. Chapter 6 summarizes the conclusions and suggests future work.

THIS PAGE INTENTIONALLY LEFT BLANK

CHAPTER 2:
Background

2.1 Literature Review

There have been numerous theoretical, numerical, and experimental studies of wave-induced loads on submerged bodies. Some of the earliest work involved theoretical studies using potential flow theory. A sample of these theoretical studies include Dean [4], Ursell [5], [6], and Ogilvie [7], who determined expressions for linear and nonlinear forces on a two-dimensional circle, and Cummins [8] and Wilmott [9], who derived expressions for linear and nonlinear forces on a three-dimensional body with a circular cross section. Studies using numerical simulations have built upon the theoretical studies and allowed for the inclusion of different input geometries. A sample of these numerical studies include Pinkster [10], Crook [11], Ananthakrishnan and Zhang [12], Fang et al. [13], and Carrica et al. [14]. Many of the experimental studies have been conducted to verify results from previous theoretical and numerical studies, such as Cummins [15], Henry et al. [16], and Pinker [10]. Additional experimental studies examining wave-induced loads on underwater vehicles include Khalil [17], Sayer [18], and Inoue et al. [19]. More recently, a number of numerical and experimental studies have been conducted at the Naval Postgraduate School (NPS).

2.2 Previous NPS Work

Previous work related to this research has been conducted at NPS by Jones [20], Turner et al. [21], Turner [22], Whitmer [23], and Suriben [24].

Jones [20] conducted a numerical study using a computational fluid dynamics model to predict loads experienced by a submerged body near the surface. He then compared the first-order linear portion of the loads to actual linear loads measured during an experimental study. The experimental study used a submerged body in the shape of a rectangular prism with a square cross section which was held fixed at a single nondimensional depth of 2.0. Loads for the study were induced by generating single-component waves with nondimensional wavelengths ranging from 0.5 to 2.2 and an amplitude of one inch. After comparing the

results of the two studies, he concluded that the model could be used to closely predict first-order loads for nondimensional wavelengths between 1.125 and 1.375. However, he noted that the model overpredicted loads for nondimensional wavelengths greater than 1.5 and suggested further refinement of the model through additional studies.

Turner et al. [21] conducted an experimental study that evaluated a closed-form analytical solution for predicting the first-order loads from linear inviscid flow on a slender body of revolution at near-surface depths. The study used a submerged body in the shape of a right circular cylinder with hemispherical end caps which was held fixed at nondimensional depths of 1.0 and 2.0. Loads for the study were induced by generating single-component waves with nondimensional wavelengths ranging from 0.5 to 2.2 and an amplitude of one inch. After comparing the predicted loads and actual loads, Turner et al. concluded that the analytical solution reasonably predicts first-order loads on a slender body of revolution for nondimensional wavelengths greater than 1.0 and for sufficiently deep depths. However, Turner et al. notes that the analytical solution underpredicts the vertical force and pitch moment for nondimensional wavelengths less than 1.0 and for shallow depths. The study hypothesizes that the underprediction of the vertical force and pitch moment resulted from the wave profile changing as it passed over the submerged body.

Expanding on his work in Turner et al. [21], Turner [22] examined the effects of hull cross section on first-order loads. The study used submerged bodies in multiple shapes including a right circular cylinder with hemispherical end caps, a rectangular prism with a square cross section and semi-cylindrical end caps, and a rectangular prism with a rectangular cross section and semi-cylindrical end caps which was used in both horizontal and vertical orientations. The submerged bodies were held fixed at nondimensional depths of 1.0, 1.5, 2.0, and 3.0 during the study. Loads for the study were induced by generating single-component waves with nondimensional wavelengths ranging from 0.5 to 2.0 and an amplitude of one inch. The results of the study showed no significant difference between the loads experienced by the submerged bodies with circular, square, and vertically-oriented rectangular cross sections. However, the results did show a significant difference in the loads experienced by the submerged body with a horizontally-oriented rectangular cross section. Turner concludes that cross-sectional geometry does affect the first-order loads experienced at near-surface depths, and he also notes that the loads experienced decrease exponentially as depth increases.

Utilizing the same submerged body as Turner et al. [21], Whitmer [23] examined whether linear superposition of single-component waves could be used to predict first-order loads in complex seaways. The submerged body was held fixed at a nondimensional depth of 2.0 during the study. Loads for the study were induced by generating single-component waves with nondimensional wavelengths ranging from 0.5 to 2.0 and amplitudes of 0.25, 0.50, 0.75, and 1.0 inches. Whitmer used linear superposition of these single-component waves to predict multi-component waves which he then tested. After comparison of the linear superposition results and the multi-component wave results, he concluded that linear superposition is a valid theory for predicting first-order loads on a shallowly submerged body in complex seaways.

Suriben [24] conducted an experimental study that examined the effects of viscous flow on the first-order loads experienced by a shallowly submerged body at speed and compared the results to the analytical solution for inviscid flow used by Turner et al. [21]. Two submerged bodies with right circular cylindrical shapes were used in the experiment, one with hemispherical end caps and one with flat-faced end caps. The submerged bodies were run at nondimensional depths of 1.0 and 2.0 and speeds of 1.25, 2.5, and −2.5 feet per second during the study. Loads for the study were induced by generating single-component waves with nondimensional wavelengths ranging from 1.0 to 4.125 and an amplitude of one inch. The results of the study showed that the analytical solution for inviscid flow did not accurately predict first-order loads for viscous flow but did follow the same trends in behavior with respect to depth, wavelength, and speed. Suriben also noted that results for both submerged bodies were similar except for an increased pitch moment on the submerged body with flat-faced end caps, which indicated a relationship between pitch moment and the size and location of the separation region.

Building upon the aforementioned research, this study uses similar wave environments and a free-floating, self-propelled ROV instead of the fixed models previously used. The goal of which is to examine the effect of wave-induced loads on pitch motion and depth changes. It was originally intended for this study to use an AUV with a torpedo-like shape to build upon the previous research using right circular cylinders with hemispherical end caps. However, a lack of technical support for the system acquired precluded its use in this research, and an inability to acquire a similar system within the time constraints for completing this research resulted in the use of an ROV that was already on hand.

THIS PAGE INTENTIONALLY LEFT BLANK

CHAPTER 3:
Experimental Setup and Procedure

3.1 Experimental Setup

3.1.1 Wave Tank

The experiments were conducted using a tow tank with wave making capability located in the NPS Hydrodynamics Lab. The tank, shown in Figure 3.1, has a length of 36 feet, a width of three feet, a height of four feet, and a water depth of approximately three feet. It is constructed of aluminum and sits upon two steel I-beams for support. Plexiglas panels line one side of the tank for observation within the tank during testing. At one end of the tank is a wavemaker system and at the opposite end is a wave-absorbing beach.

Figure 3.1. Side view of the NPS Hydrodynamics Laboratory tank.

3.1.2   Wavemaker and Wave-Absorbing Beach

The desired wave environment was produced using the wavemaker system shown in Figure 3.2. As seen through the Plexiglas panel in Figure 3.2, the wavemaker utilizes a wedge-shaped plunger which generates waves through an oscillating vertical motion. The wedge has an interior angle of 35 degrees from vertical and is two feet in height with a width slightly under three feet to fit the width of the tank. It is supported by a frame and two vertical guide rails constructed from prefabricated 80/20 T-slotted aluminum. When moving along the vertical guide rails, the frame is guided through slots by Teflon roller bearings. The motion of the wedge is driven by a Moog Animatics SM34165MT SmartMotor, a ModuSystems MAC-2TC Pulse/Dir motion controller, and an E-Drive L-TAC LS ball screw linear actuator (LS204-24).
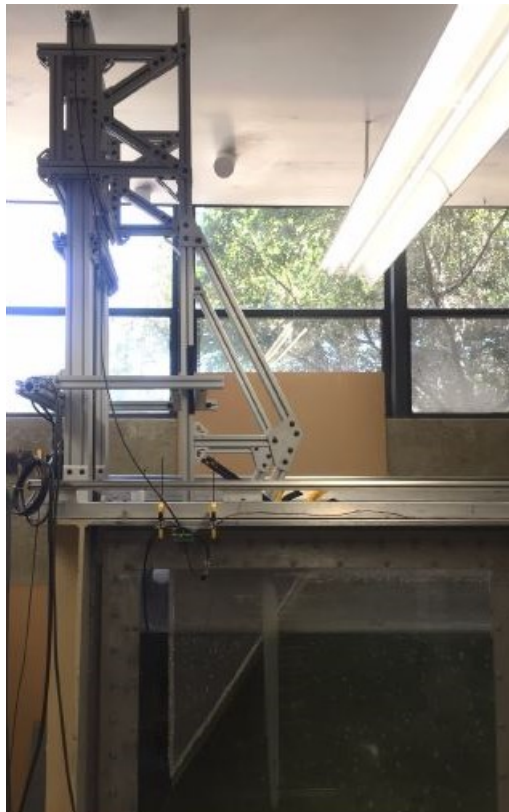
Figure 3.2. Side view of the wavemaker system. Source: [25].

The wave-absorbing beach at the opposite end of the tank from the wavemaker, shown in Figure 3.3, is designed to reduce the energy of reflected waves so that the desired wave environment is present throughout the tank. It is comprised of two perforated acrylic sheets that are four feet in length and fit the width of the tank. The two acrylic sheets are layered on top of each other and are suspended at a 12 degree incline.

Figure 3.3. Wave-absorbing beach used to reduce the energy of reflected waves.

3.1.3   Software and Instrumentation

Generating a desired wave was accomplished by first determining the required amplitude, frequency, and phase of the sine function used to describe the oscillatory motion of the wedge. The wavemaker was then programmed with these parameters using the ModuSystems Snap2Motion software which interfaced with the motion controller for the wavemaker.

Wedge motion and wave elevation were measured using four Senix ToughSonic 14 ultrasonic sensors. One ultrasonic sensor was located at the top of the wavemaker, as shown in Figure 3.4, for measuring wedge motion, and three ultrasonic sensors were suspended over the wave tank, as shown in Figure 3.5, to measure wave elevation. Analog voltage readings from the ultrasonic sensors, which were later converted to physical measurements, were recorded using a laptop running MATLAB via a National Instruments USB-6363 data acquisition board.
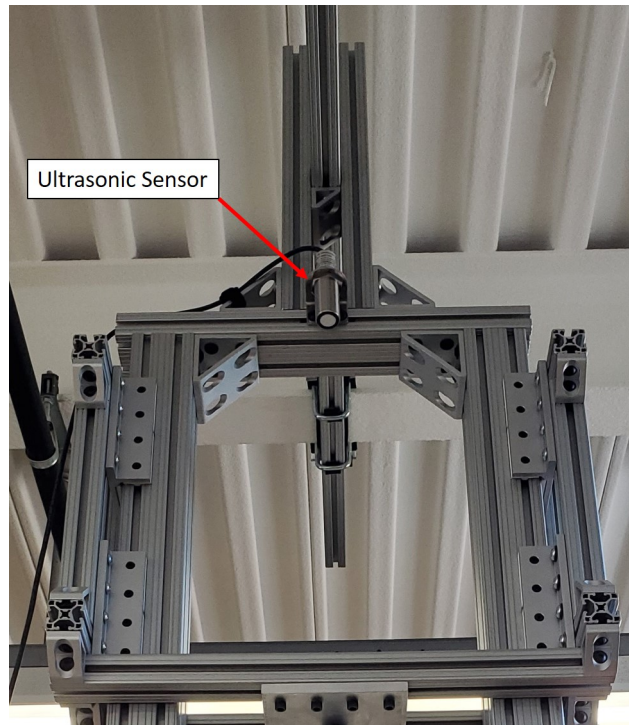
Figure 3.4. Senix ToughSonic 14 ultrasonic sensor located on the wavemaker for measuring wedge motion.
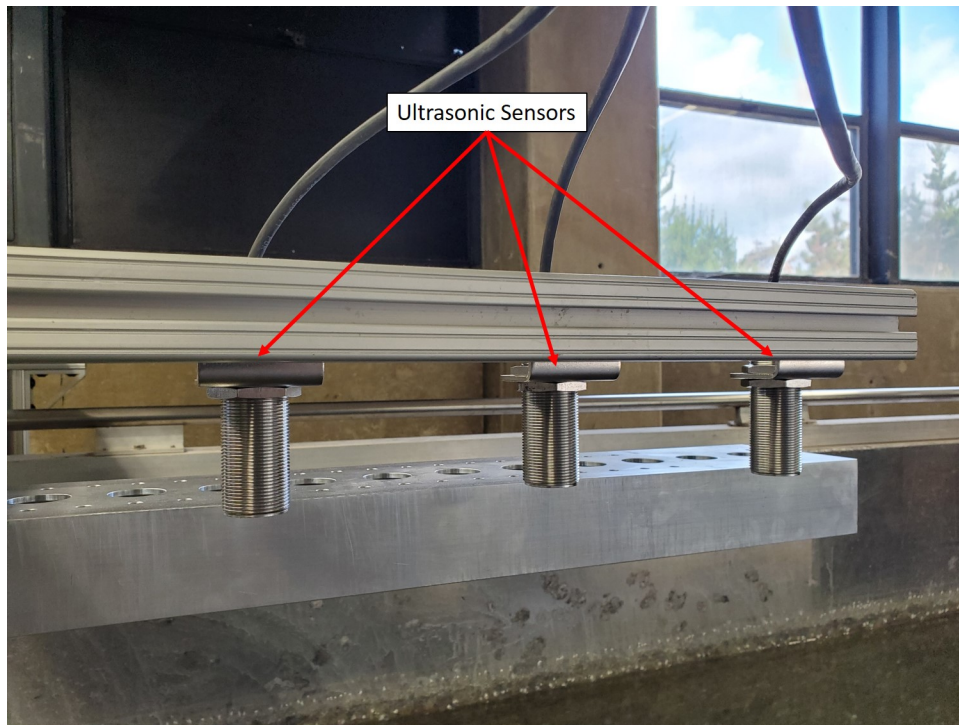
Figure 3.5. Senix ToughSonic 14 ultrasonic sensors located over the wave tank for measuring wave elevation.

3.1.4 ROV

The ROV used in this study was a Blue Robotics BlueROV2, shown in Figure 3.6, in a six-thruster vectored configuration. It is intended for use as either a work class or a research class ROV, and it utilizes a modular design capable of expansion for accessories and custom modifications. The frame is constructed of high-density polyethylene, and the two watertight enclosures, one for housing the electronics and one for housing the battery, are constructed of acrylic tubes with aluminum end caps. Buoyancy is adjusted using four fairings with R-3318 urethane foam mounted to the top of the frame and lead ballast weights mounted to the bottom of the frame. For this study, the ROV was assembled so that it would be negatively buoyant and rest at the bottom of the tank between runs. Technical specifications for the ROV as assembled are listed in Table 3.1.
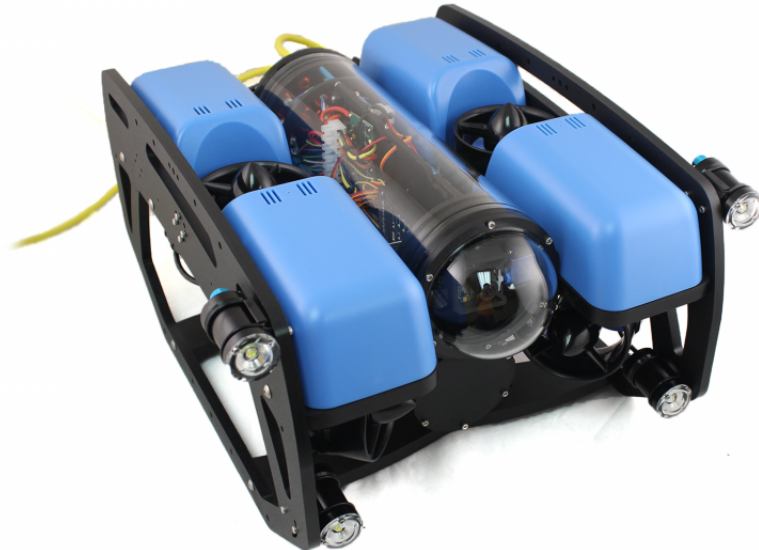
Figure 3.6. Blue Robotics BlueROV2 in a six-thruster vectored configuration.
Source: [26].

Table 3.1. BlueROV2 Technical Specifications. Adapted from [26].

Length	18 in
Width	13.3 in
Height	10 in
Equivalent Diameter	13 in
Weight	22 lb
Maximum Rated Depth	330 ft
Maximum Forward Speed	3 knots
Forward Bollard Thrust	20 lbf
Vertical Bollard Thrust	16 lbf
Lateral Bollard Thrust	20 lbf

In the six-thruster vectored configuration, the ROV uses six Blue Robotics T200 thrusters, three with clockwise propellers and three with counter-clockwise propellers, arranged with four horizontal thrusters and two vertical thrusters as shown in Figure 3.7. In Figure 3.7, the red triangle shows the front of the ROV, the thrusters with counter-clockwise propellers are green, and the thrusters with clockwise propellers are blue.
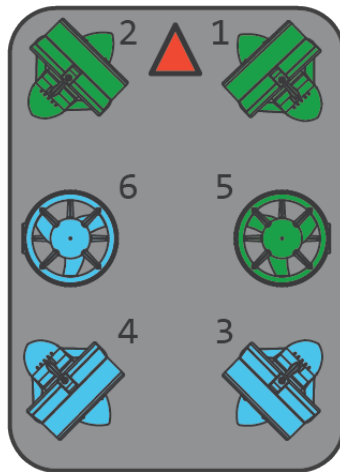
Figure 3.7. Diagram of the BlueROV2 thruster configuration. Source: [27].

Inside the electronics enclosure is a Raspberry Pi Model B computer and a Pixhawk 1 flight controller running ArduSub control software. Sensors on the Pixhawk flight controller include a ST Micro L3GD20H three-axis gyroscope, a ST Micro LSM303D three-axis accelerometer and magnetometer, an Invensense MPU-6000 three-axis accelerometer and gyroscope, and a MEAS MS5611 internal barometer. There is also a Blue Robotics Bar30 pressure sensor utilizing a Measurement Specialties MS5837-30BA pressure sensor with a 0.2 mbar resolution. Additional equipment used for operating the ROV included a Fathom tether, a Fathom-X tether interface board, a laptop running QGroundControl ground control station software, and a XBox One controller.

There are three preset dive modes for operating the ROV: manual mode, stabilize mode, and depth hold mode. In manual mode, the ROV does not utilize feedback stabilization, heading holding, or depth holding and only outputs motor controls based on controller inputs. In stabilize mode, the ROV stabilizes roll and maintains heading unless commanded to turn. In

depth hold mode, the ROV maintains depth unless commanded to dive or ascend and also stabilizes roll and maintains heading unless commanded to turn. In addition to the three preset dive modes, the ROV is capable of an input hold where the current controller input is maintained until disabled.

As is, the ROV does not have a positioning system that would enable speed measurements, which prevented the use of a specified speed throughout all of the forward speed runs. In an attempt to create a repeatable speed, the controller input gain was reduced to a setting where the maximum controller input resulted in a speed that allowed the ROV to transit the length of the tank in the same length of time as the desired run duration. This also allowed for the maximum controller input to be used with the input hold function to create a repeatable speed for each forward speed run.

3.2   Experimental Procedure

Prior to each run, the parameters for the desired wave environment were programmed into the wavemaker, and the ROV was centered at the bottom of the wave tank just in front of the wave-absorbing beach on the opposite end from the wavemaker. The ROV was then placed in manual mode and armed in QGroundControl to begin recording sensor data to a log file. For approximately 30 seconds, the ROV was held at the bottom of the tank to determine the sensor offsets while not in motion. After the initial 30 seconds, the ROV was raised to the desired depth and placed in depth hold mode. Once the ROV was positioned, the wavemaker was started. Data collection for the waves was started once the waves had propagated past the ultrasonic sensors positioned over the tank. For zero speed runs, the ROV was not given any controller inputs except to help maintain its lateral position in the center of the tank to avoid collision with the walls of the tank. At the end of the run, the ROV was disarmed to cease writing data to the log file and the wavemaker was stopped. For forward speed runs, a forward speed input was given after the waves had reached the ROV. The forward speed was maintained using the input hold function, and additional inputs were given to maintain its lateral position in the center of the tank. Once the ROV had reached the end of the tank, it was disarmed and the wavemaker was stopped. Each set of test conditions was repeated three to five times and the same set of wave environments were used for both zero speed and forward speed runs.

CHAPTER 4:
Data Collection and Reduction

4.1 Wave Data

Voltages from the ultrasonic sensors were collected using the data acquisition board and a laptop running MATLAB. A custom MATLAB script recorded the data using a sampling time of 60 to 75 seconds and a sampling rate of 24 Hz. The script also provided real-time plots of each sensor channel for monitoring during the run. Raw data for each run was saved into a .dat file for data reduction.

At the beginning of each data collection session, a zero file was obtained for calm water. The zero file was used to calculate the sensor offset for each channel which was removed from subsequent runs during that session. A gain for each sensor was then applied to the voltage readings for conversion to wave elevation in physical units of inches.

A fast Fourier transform was used to verify that the oscillation frequency of the wedge matched the desired frequency. This wedge frequency is equal to the wave frequency, ω, of the generated wave. The wavenumber, k, was then estimated using the finite depth third-order dispersion relationship

$$\omega^2 = gk\varphi\left(1 + \frac{9 - 10\varphi^2 + 9\varphi^4}{8\varphi^4}(ka_w)^2\right) \tag{4.1}$$

where g is gravitational acceleration, $\varphi = \tanh(kH)$ where H is water depth, and a_w is wave amplitude. Wavelength, λ, was then determined from the wavenumber definition

$$k = \frac{2\pi}{\lambda}. \tag{4.2}$$

A least-squares fit of the wave time history data, $\eta(x,t)$, was then performed using the functional relationship

$$\eta(x,t) = \sum_{i=1}^{n}\left(A_i\cos(k_ix - \omega_it) + B_i\sin(k_ix - \omega_it)\right) + C \tag{4.3}$$

where i is the wave component, n is the total number of wave components, A_i and B_i are the cosine and sine components of the linear first-order amplitude, x is the sensor location relative to a common origin, and C is the mean value of the wave elevation signal.

Wave amplitude and phase angle, $\phi_{w,i}$, were then calculated from the sine and cosine components using the trigonometric identity

$$a_{w,i} \sin\left(\omega_i t + \phi_{w,i}\right) = A_i \cos\left(\omega_i t\right) + B_i \sin\left(\omega_i t\right) \tag{4.4}$$

where amplitude is given by

$$a_{w,i} = \sqrt{A_i^2 + B_i^2} \tag{4.5}$$

and phase angle is given by

$$\phi_{w,i} = \tan^{-1}\left(\frac{B_i}{A_i}\right). \tag{4.6}$$

The spatial position term in Equation 4.3 allowed each phase angle to be referenced to a common origin in a single coordinate system. By utilizing a single coordinate system, the average phase angle of each wave component could be estimated by averaging the phase angle calculated from each sensor.

For single-component waves, wave height, h, was estimated using the third-order Stokes wave elevation approximation

$$h = 2a_w \left(1 + \frac{3}{8}k^2 a_w^2\right). \tag{4.7}$$

A simpler approximation of wave elevation is to use twice the wave amplitude; however, the third-order Stokes wave elevation approximation was used to account for steep waves at shorter wavelengths. This was shown to provide an accurate approximation of wave elevation for steep waves by Klamo et al. [25].

For two-component waves, a single wave height was not identified, as it was not the parameter of interest, and Equation 4.7 was not utilized. Instead, the wave amplitude of each of the underlying wave components was the parameter of interest, and these were determined from Equation 4.5.

4.2 ROV Data

Sensor data for the ROV was saved to DataFlash logs as .bin files using onboard memory. At the end of each data collection session, the log files were downloaded to a laptop via QGroundControl and then converted to .mat files. A custom MATLAB script was then used for data reduction. The first step of which was to generate a time history plot of pitch and depth. This plot was used to identify the different portions of each run as described in Section 3.2. Figure 4.1 provides an example of a time history plot with the different portions of each run identified. The run conditions for this example were forward speed with a two-component wave. The first point shows the start of the 30-second period at the beginning of each run where the ROV remained at the bottom of the tank. Data from this portion was used to determine sensor offsets which were later removed from the sensor channels. The second point shows when the ROV was raised to the desired depth, and the third point shows when the waves reach the ROV. Data from these portions were disregarded and not used for analysis. The fourth point shows where the ROV begins moving forward and was selected as the starting point for data analysis of the run.

For pitch, the angular rate channels were integrated to determine angular position. The angular position for the selected starting point was set as the initial condition. Using this method, the absolute angular positions were uncertain; however, the primary focus is on the oscillation amplitude of the pitch motion which is unaffected by the absolute initial pitch angle. This would simply cause a shift in the pitch angle time history but not alter the amplitude of the oscillating signal. Figure 4.2 shows an example time history plot of pitch after data reduction.
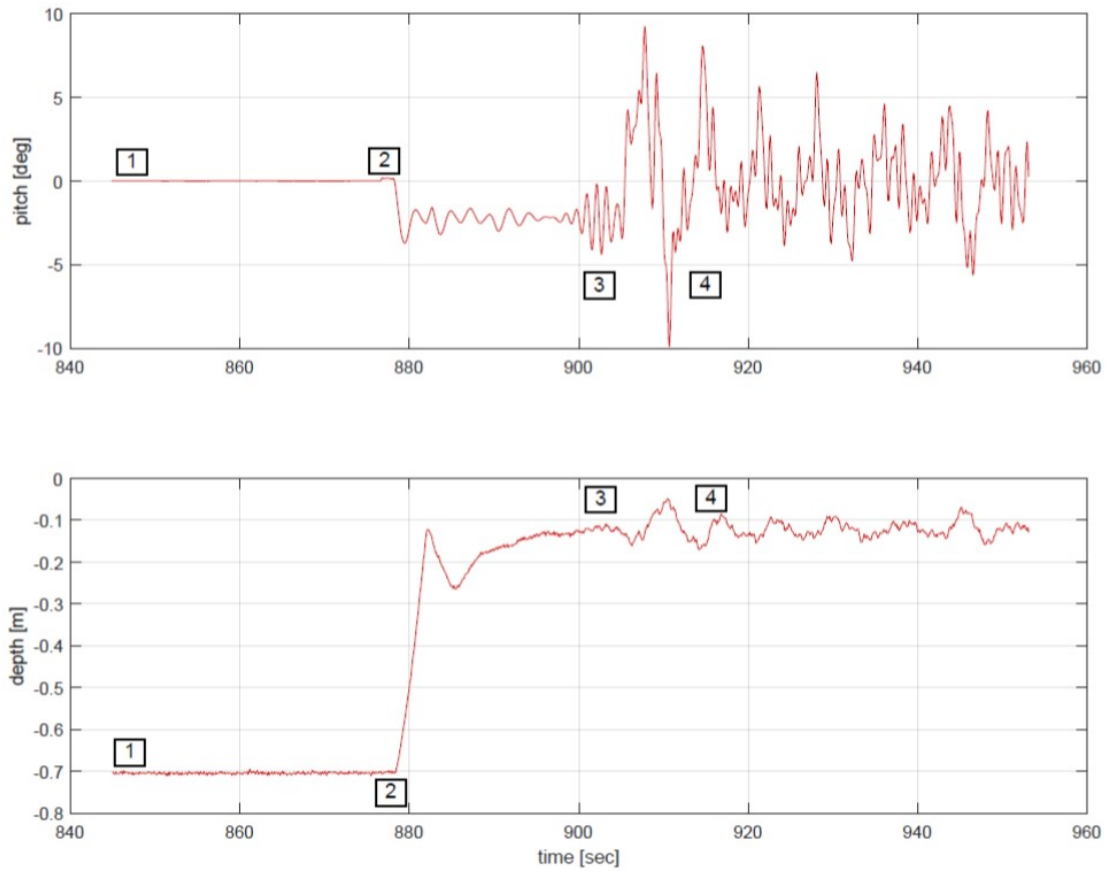
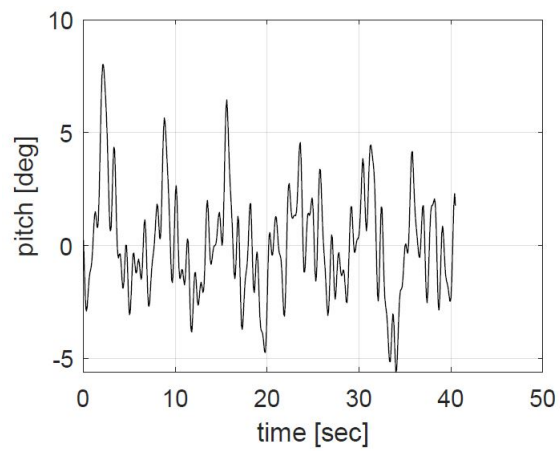Figure 4.1. An example time history plot of pitch and depth.

Figure 4.2. An example time history plot of pitch modified for data analysis.

For depth, the ROV used internal calculations to determine depth from pressure sensor readings, and data reduction was performed so that the selection of depth data corresponded to the pitch data selected. Since the ROV has the capability to control its depth while in the depth hold mode, additional data from the vertical thrusters was also obtained to examine the thruster response as the ROV attempted to maintain depth. Pulse width modulation signals from the electronic speed controllers used to control the thrusters were converted to thruster revolutions per minute (RPM) using a curve fit created by Blue Robotics [28] and shown in Equation 4.8

$$y = -3.54316527456654 \cdot 10^{-5}x^3 + 0.158465413759068x^2$$
$$-223.390468750005x + 98127.0694489722$$

(4.8)

where y is the thruster RPM and x is the pulse width modulation signal.

Pitch, depth, and thruster data were then analyzed in the frequency domain using a power spectral density (PSD) plot and a narrow frequency search window to identify frequencies of interest. These frequencies were those with energy maximums and included wave encounter frequencies, two-component wave frequency differences, and natural system frequencies. Figure 4.3 shows an example pitch PSD plot for a run using a two-component wave with the frequencies of interest labeled. In the figure, solid lines represent frequencies of interest while dashed lines represent the frequency search windows used for identification.

To determine the response amplitude for pitch, depth, and thruster RPM corresponding to the frequencies of interest, a curve fit was performed using the functional relationship

$$f(t) = \sum_{i=1}^{n} \left(A_i \cos(\omega_i t) + B_i \sin(\omega_i t) \right) + C$$

(4.9)

where i is the response component, n is the total number of response components, A_i and B_i are the cosine and sine components of the response amplitude, ω_i is the frequency of interest, and C is the mean value of the response amplitude. The cosine and sine components of the response amplitude where then used to calculate the response amplitude, a_i, using Equation 4.10.

$$a_i = \sqrt{A_i^2 + B_i^2}$$

(4.10)

21
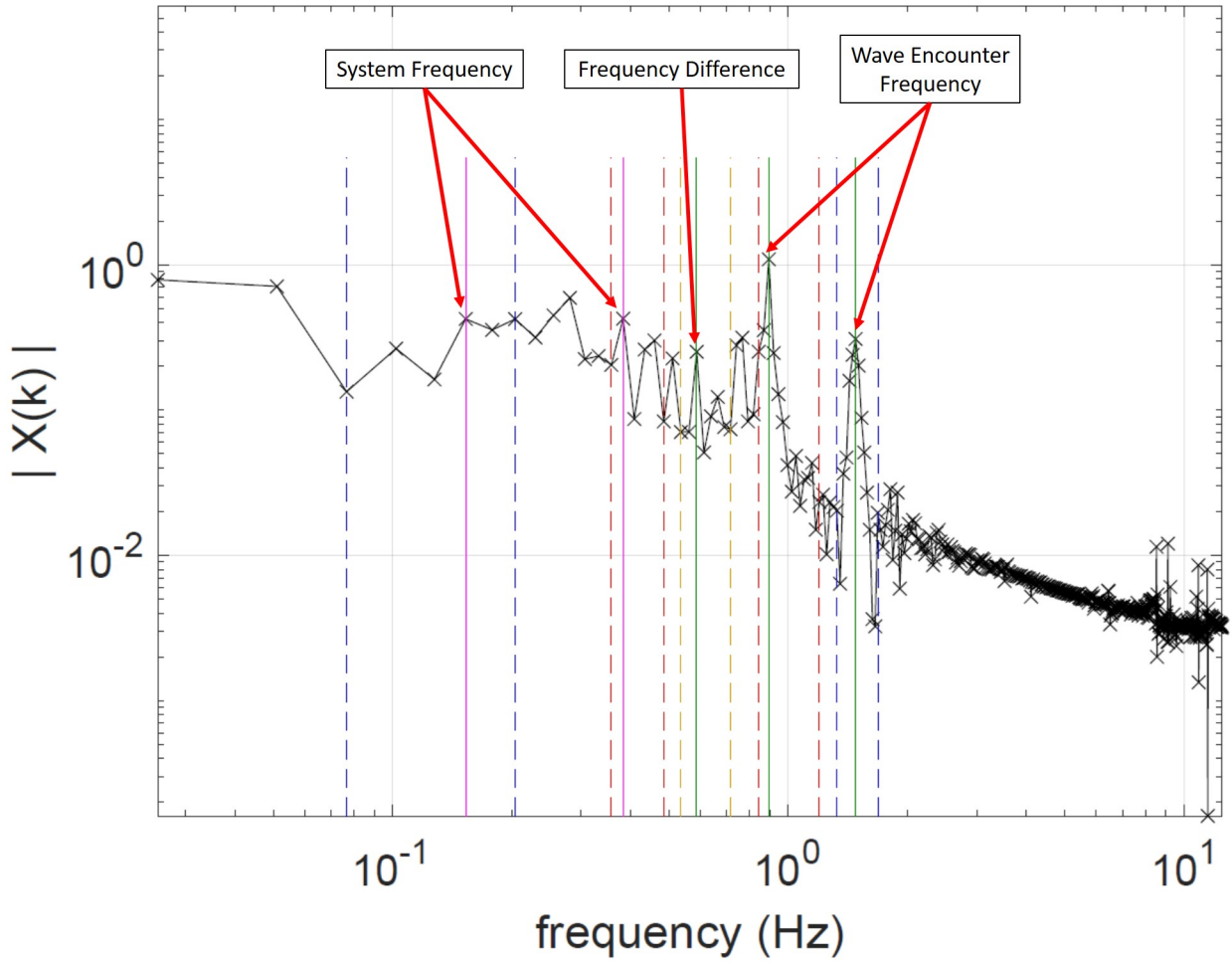
Figure 4.3. An example time history plot of pitch modified for data analysis.

The response frequencies and amplitudes for the control runs were used to establish a baseline for ROV performance and then compared to the response frequencies and amplitudes in wave environments.

Finally, the wave encounter frequencies identified were used to estimate ROV speed through the relationship between wave encounter frequency, ω_e, wave frequency, ω, and velocity, u, given by

$$\omega_e = uk \cos(\mu) + \omega \qquad (4.11)$$

where μ is the relative wave heading which is zero for head seas.

4.3   Vehicle Sensor Verification

Prior to data collection, a series of simple tests were done to verify sensor readings and orientation for the ROV. To verify pitch data, the ROV was pitched downward 90 degrees for five seconds, leveled for five seconds, pitched upward 90 degrees for five seconds, and then leveled again. Figure 4.4 shows a plot of the pitch test and verifies the accuracy of the sensor data. To verify depth data, the ROV was lowered to the bottom of the tank and then raised to the surface three times. Figure 4.5 shows a plot of the depth test and verifies the accuracy of the depth sensor. Thruster data from the depth test was also used to verify which thrusters were in the vertical orientation and is also shown in Figure 4.5.
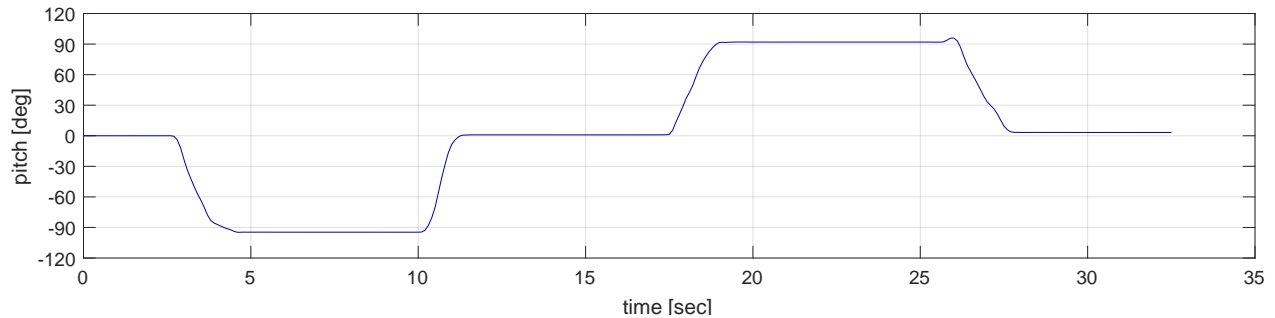

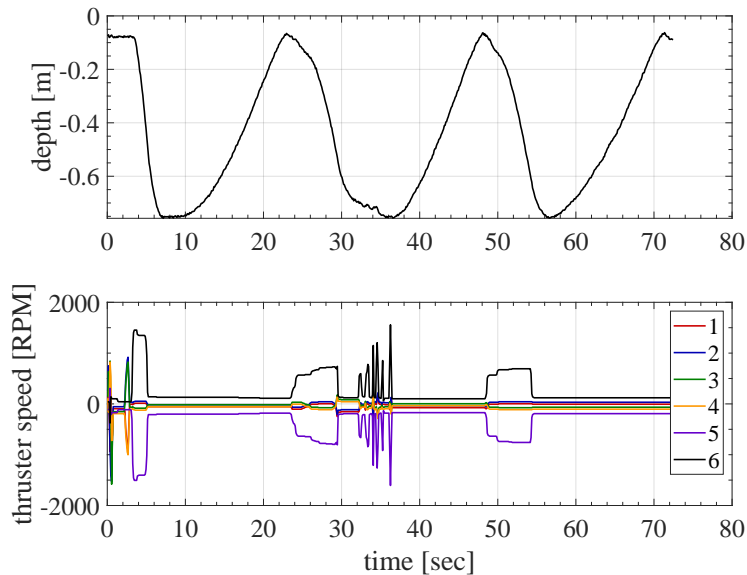Figure 4.4. Sensor verification for pitch.

Figure 4.5. Sensor verification for depth and thrusters.

4.4 Test Conditions and Wavemaker Settings

Throughout the experiment, an approximate centerline depth of eight inches, corresponding to a nondimensional depth of about 0.6, was used. The single-component waves generated used a wave amplitude of one inch with nondimensional wavelengths of 1.0, 2.0, 2.5, , 4.0, and 5.0. For the two-component waves generated, the second wave used a wave amplitude of 0.5 inches with nondimensional wavelengths of 1.5, 2.0, and 5.0. Table 4.1 lists the test conditions used with each test condition being repeated three to five times.

To determine the wavemaker settings required to generate the desired wave conditions in the test matrix, a transfer function was used. Inputs for the transfer function included ROV length, tank water depth, and desired wave height. The transfer function was then applied to obtain the required wedge amplitude for a given nondimensional wavelength. An example of the wavemaker settings used is shown in Figure 4.6.

Table 4.1. Test conditions used for data collection.

Depth	Forward Speed	Wave 1 Composition			Wave 2 Composition		
D [in]	[Y=1/N=0]	a_w [in]	λ [ft]	λ/L	a_w [in]	λ [ft]	λ/L
8	0	0	0	0	0	0	0
8	0	1	1.5	1	0	0	0
8	0	1	3.75	2.5	0	0	0
8	0	1	7.5	5	0	0	0
8	0	1	3.75	2.5	0.5	2.25	1.5
8	0	1	7.5	5	0.5	3	2
8	1	0	0	0	0	0	0
8	1	1	1.5	1	0	0	0
8	1	1	3	2	0	0	0
8	1	1	3.75	2.5	0	0	0
8	1	1	6	4	0	0	0
8	1	1	7.5	5	0	0	0
8	1	1	3.75	2.5	0.5	7.5	5
8	1	1	7.5	5	0.5	3	2

	water depth =	3	(ft)			Danger P2P	6.5	inches	a_wave / a_wedge = Af^2+Bf+C	
	max wave length =	6	(ft)				165.1	mm	A =	-0.2253755
	Desired Wave Height =	2	(inches)						B =	1.5621619
	model length =	18	(inches)						C =	-0.5258382

	desired lambda / L	required wave length	steepness	k	sigma	omega	freq	wedge actual	wedge CMD	ITERATED wedge CMD
	(---)	(ft)	(---)	(1/ft)	(---)	(rad/s)	(Hz)	(in)	(mm)	(mm)
1	1.0000	1.500	9	4.18879	1	12.295994	1.957	0.599471184	30.453	
2	1.5000	2.250	13.5	2.79253	1	9.73202591	1.549	0.739044763	37.543	
3	2.0000	3.000	18	2.0944	0.99999	8.33290339	1.326	0.869920005	44.192	
4	2.5000	3.750	22.5	1.67552	0.99991	7.41312813	1.180	0.996481414	50.621	
5	3.0000	4.500	27	1.39626	0.99954	6.7461989	1.074	1.121547479	56.975	
6	3.5000	5.250	31.5	1.1968	0.99848	6.23143473	0.992	1.247226589	63.359	
7	4.0000	6.000	36	1.0472	0.99627	5.8158826	0.926	1.375436368	69.872	
8	4.5000	6.750	40.5	0.93084	0.99252	5.46868733	0.870	1.508097287	76.611	
9	5.0000	7.500	45	0.83776	0.98696	5.17067005	0.823	1.647192824	83.677	
10	5.5000	8.250	49.5	0.7616	0.97949	4.90937953	0.781	1.794797438	91.176	
11	6.0000	9.000	54	0.69813	0.97012	4.67646345	0.744	1.95311326	99.218	

Figure 4.6. An example of the wavemaker settings used.

THIS PAGE INTENTIONALLY LEFT BLANK

CHAPTER 5:
Results and Analysis

5.1   Control Runs

Analysis was first conducted on the control runs to identify which frequencies were present while in a calm water environment. For the control runs with zero speed, the maximum peak in the pitch PSD plot corresponded to a frequency of about 0.4 Hz. For the control runs with forward speed, the maximum peak in the pitch PSD plot corresponded to a frequency of about 0.1 Hz. Furthermore, the second largest peak for the zero speed and forward speed control runs corresponded to frequencies of about 0.1 and 0.4 Hz, respectively. These two frequencies appear to be natural system frequencies inherent to the BlueROV2 as it operates. An example pitch PSD plot for a forward speed control run is shown in Figure 5.1. The red dashed lines in the figure mark the peaks at the natural system frequencies.

A similar process was followed for identifying frequencies present in the depth and thruster data. Analysis of the PSD plots showed that the frequencies present matched those of the frequencies present in the pitch data. Figures 5.2 and 5.3 show examples of the PSD plots for depth and thruster RPM, respectively, for the same control run shown in Figure 5.1.
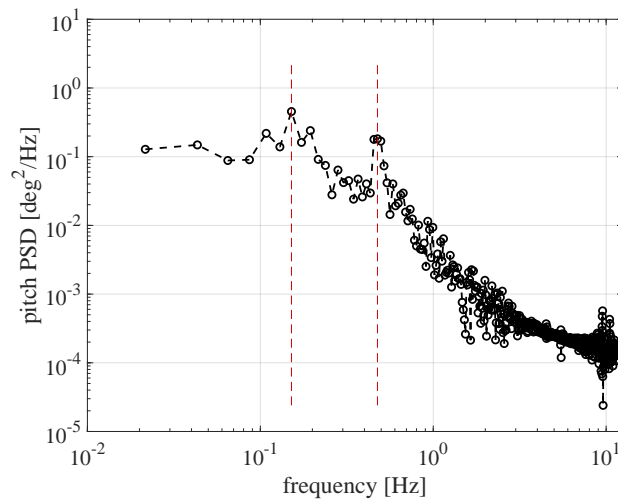

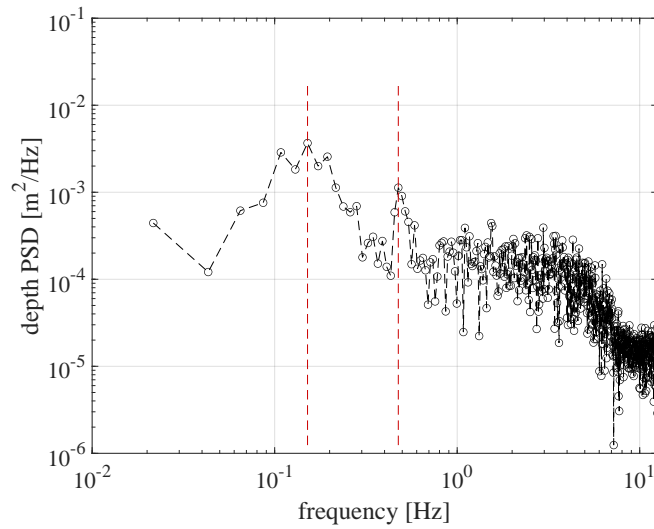Figure 5.1. An example pitch PSD plot for a forward speed control run.

27

Figure 5.2. An example PSD plot for depth using the same control run as Figure 5.1.
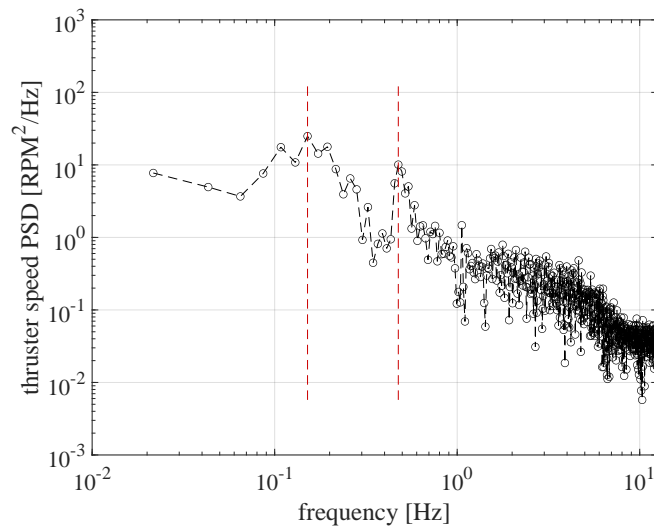

Figure 5.3. An example PSD plot for thruster RPM using the same control run as Figure 5.1.

5.2   Pitch Response

Pitch response due to linear loads acting on the ROV occurred at the wave encounter frequencies. Figure 5.4 shows a plot of pitch response amplitude per unit wave amplitude at the wave encounter frequencies as a function of nondimensional wavelength for a single-component wave at various ROV speeds. Speeds at approximately 0.9 ft/s represent runs prior to establishing a method for a repeatable speed while speeds at approximately 0.4 ft/s represent runs using the methods described in Section 3.1.4. The pitch response amplitudes were normalized for wave amplitude so as the wave amplitude increases, so to do the actual responses. A curve fit was applied to the data as a general representation of the possible behavior of the response amplitude operator (RAO) over the full range of nondimensional wavelengths. The behavior of the RAO is similar to the actual linear pitch moment experienced by a fixed model at the same depth over the same range of nondimensional wavelengths as shown in Figure 5.5. The results show that pitch response amplitude has a dependence on wavelength and that the pitch response amplitude behavior follows similar trends to the load dependence on wavelength. The results also suggest that the pitch response amplitude is a function of speed which is consistent with surface ship behavior.
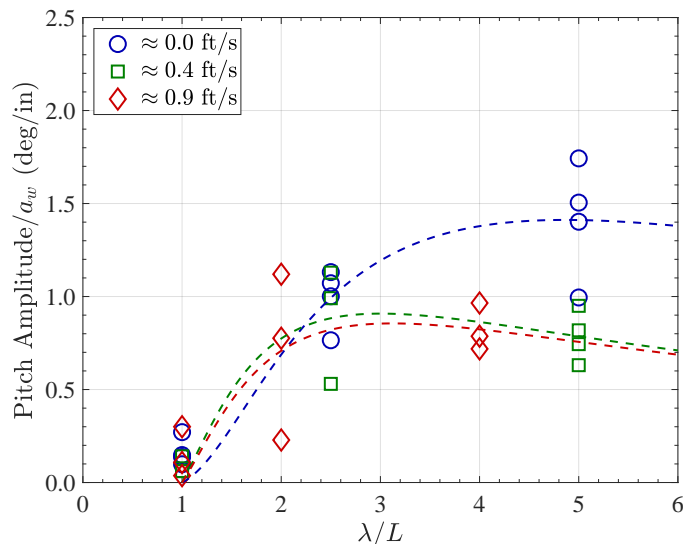

Figure 5.4. Pitch response amplitude per unit wave amplitude at wave encounter frequencies as a function of nondimensional wavelength for a single-component wave at various ROV speeds.
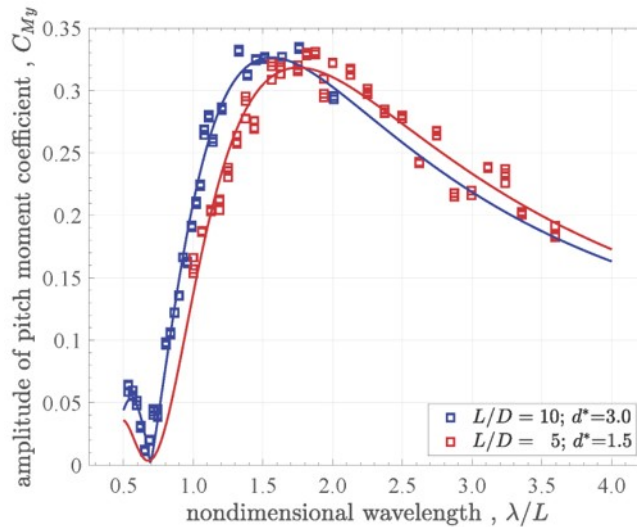
Figure 5.5. Pitch moment as a function of nondimensional wavelength for a fixed model.

A potential use of the pitch RAO is to predict pitch response in a complex seaway by summing the responses of the individual underlying wave components. Figures 5.6 and 5.7 compare the single-component wave pitch response amplitudes to the pitch response amplitudes of the underlying components for two-component waves at zero speed and at forward speeds, respectively. The single-component wave had an amplitude of one inch and the two-component wave had wave components with amplitudes of one inch and 0.5 inches. To account for the difference in wave amplitudes between the wave components, pitch response amplitude was normalized using wave amplitude. While the pitch RAO did not predict the response as accurately for the forward speeds as it did for zero speed, the results show that pitch response at single-component wave encounter frequencies can be used to predict pitch response in a complex seaway of multi-component waves by superimposing the underlying responses from single-component waves. The difference in accuracy between the zero speed and forward speed results was attributed to the lack of fidelity in speed control for the ROV. The results also confirm that the pitch RAO scales with wave amplitude. Therefore, the results of Figure 5.4 are universal and can be scaled to any wave amplitude.
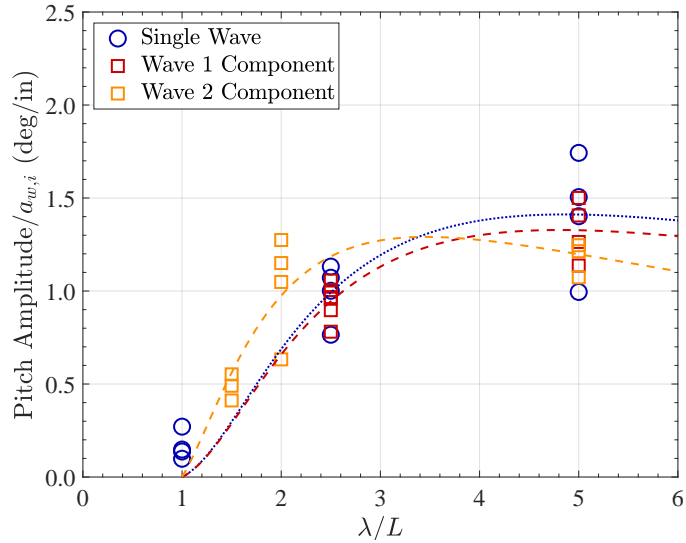
30

Figure 5.6. Pitch response amplitude per unit wave amplitude at wave encounter frequencies as a function of nondimensional wavelength for single-component and two-component waves at zero speed.
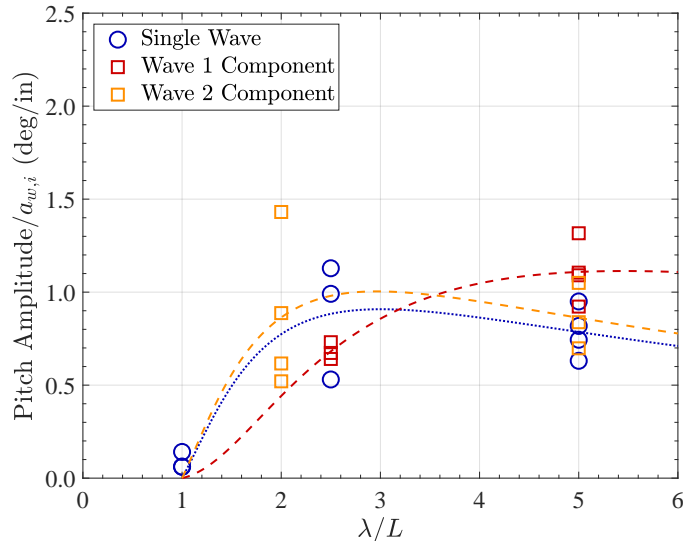

Figure 5.7. Pitch response amplitude per unit wave amplitude at wave encounter frequencies as a function of nondimensional wavelength for single-component and two-component waves at forward speed.

Pitch response due to the nonlinear loads acting on the ROV occurred at the frequency difference between wave components. Figure 5.8 shows the pitch response amplitude at the frequency difference between wave components for two-component waves at zero speed and forward speed. The pitch response amplitude was normalized by the product of the two underlying wave amplitudes. Due to the limited number of frequency differences tested, the pitch response amplitude response behavior as a function of frequency difference could not be determined.
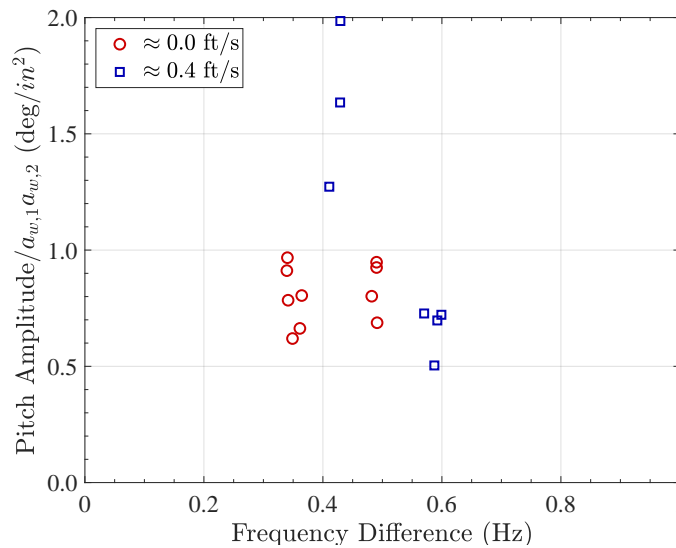

Figure 5.8. Pitch response amplitude as a function of two-component wave frequency difference for zero and forward speeds.

Pitch response at the natural system frequencies of 0.1 Hz and 0.4 Hz is shown in Figures 5.9 and 5.10, respectively. The figures show the pitch response amplitudes as a function of nondimensional wavelength for zero speed and forward speeds. While the data at speeds of 0.9 ft/s contains more scatter than the other speeds, the results show that the response is independent of wavelength and wave amplitude but dependent on speed as the response increases with speed. The scatter among the data at speeds of 0.9 ft/s was attributed to the lack of fidelity in speed control for the ROV. These results, however, are only applicable to the BlueROV2 as these frequencies are inherent to the ROV.
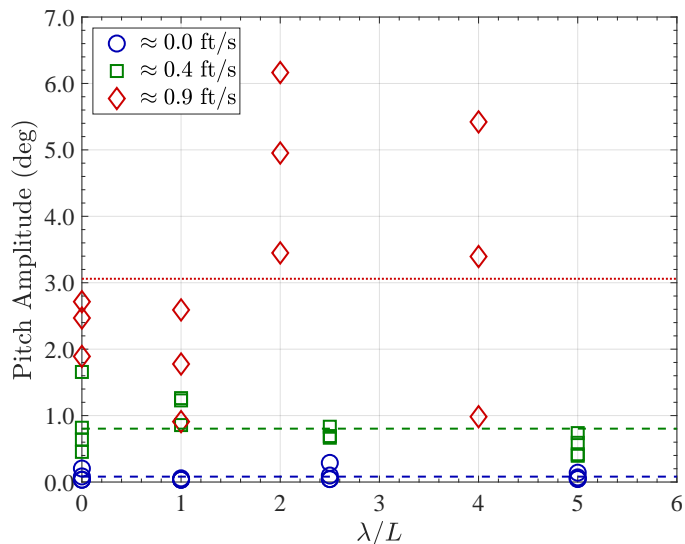
Figure 5.9. Pitch response amplitude at the 0.1 Hz system frequency as a function of nondimensional wavelength for various ROV speeds .
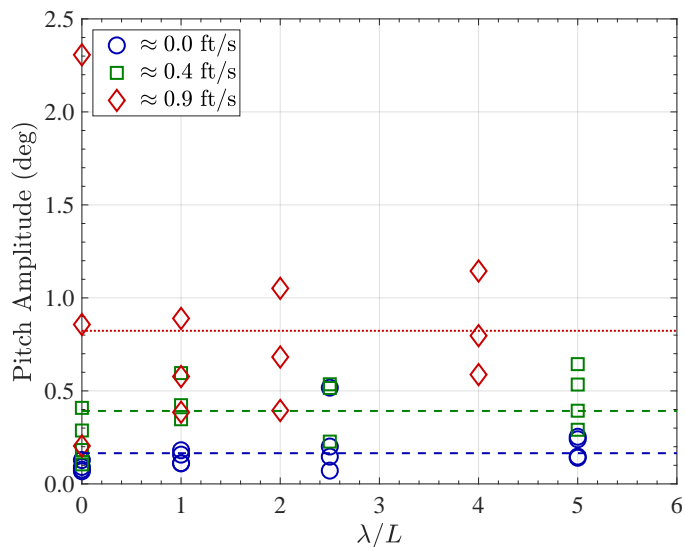

Figure 5.10. Pitch response amplitude at the 0.4 Hz system frequency as a function of nondimensional wavelength for various ROV speeds.

5.3   Depth Response

Figure 5.11 shows the depth response amplitude per unit wave amplitude at wave encounter frequencies as a function of nondimensional wavelength for various ROV speeds. The results show that there is a small dependence on wavelength. However, it is hypothesized that the lack of response is not due to a lack of vertical forcing. Rather, it is suspected that the vertical thrusters and depth hold mode provided the ROV with enough vertical control authority and response speed to overcome the periodic linear forcing. This hypothesis was based on the fact that the vertical thrusters displayed a response that was dependent on wavelength as shown in the results of the next section. Since the ROV was operated in a depth hold mode, it showed little response to not only single-component waves but also to two-component waves. Therefore, the linear response for the two-component waves and the nonlinear response at the wave component frequency differences are not shown.
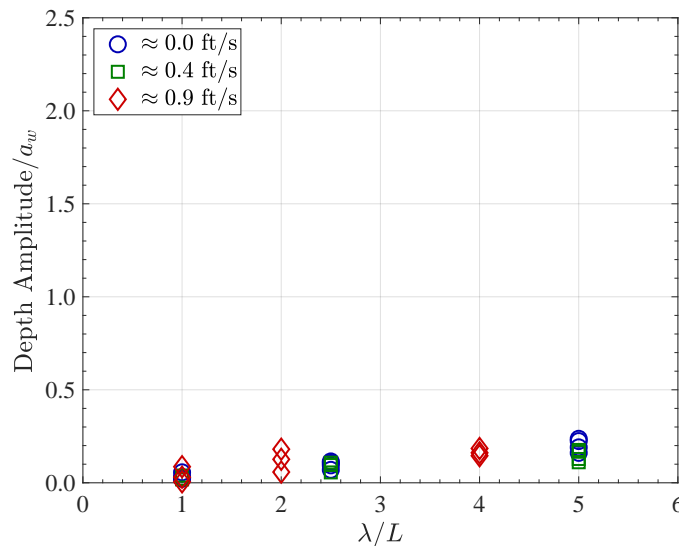

Figure 5.11. Depth response amplitude per unit wave amplitude at wave encounter frequencies as a function of nondimensional wavelength for various ROV speeds.

Figures 5.12 and 5.13 show the depth response amplitude at the natural system frequencies of 0.1 Hz and 0.4 Hz, respectively. The results are similar to the results for pitch and show that the response is independent of wavelength and wave amplitude but dependent on speed. The results also show that this behavior is more prominent at 0.1 Hz than at 0.4 Hz.
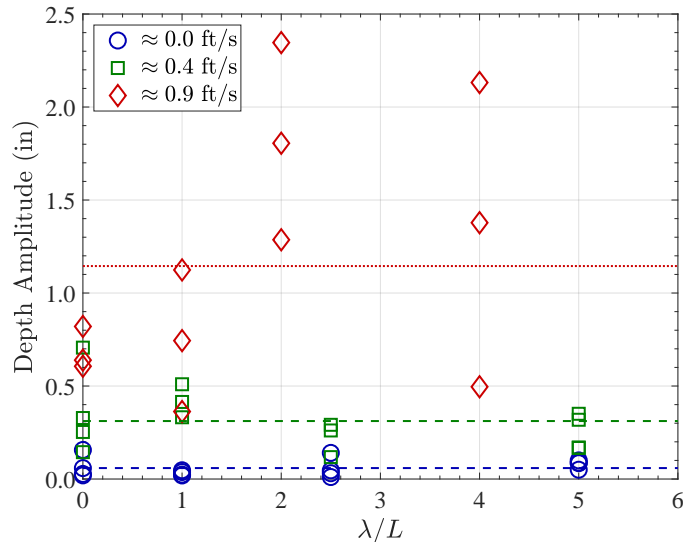
34

Figure 5.12. Depth response amplitude at 0.1 Hz system frequency as a function of nondimensional wavelength for various ROV speeds.
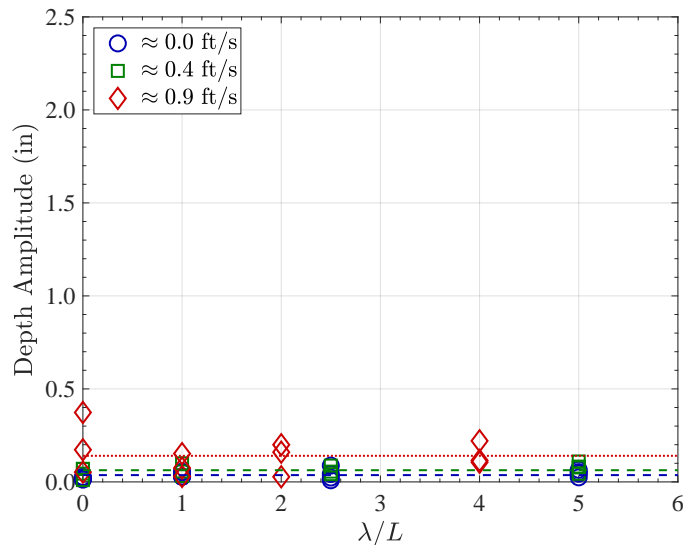

Figure 5.13. Depth response amplitude at 0.4 Hz system frequency as a function of nondimensional wavelength for various ROV speeds.

5.4 Thruster Response

Similar to the pitch response amplitude dependence on wavelength, there also appears to be a thruster response amplitude dependence on wavelength. This would account for the lack of depth response as the thrusters minimized the depth response while in the depth hold mode. The results also show that the thruster response behavior, shown in Figure 5.14, follows load dependence on wavelength as well.
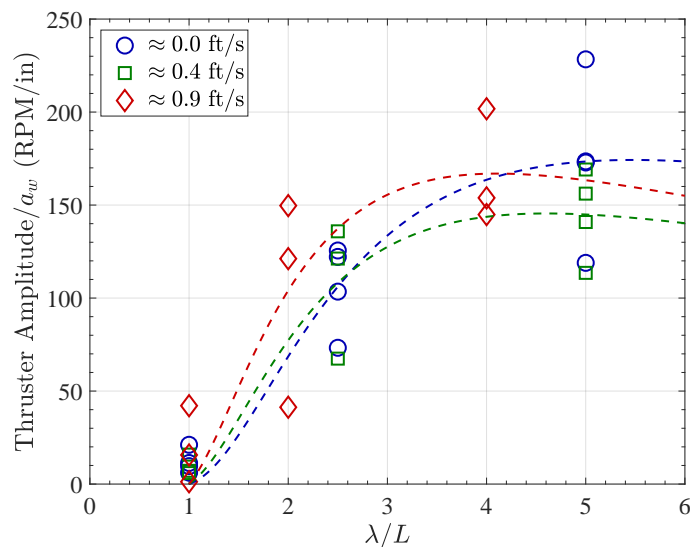

Figure 5.14. Thruster response amplitude per unit wave amplitude at wave encounter frequencies as a function of nondimensional wavelength for various ROV speeds.

The thruster response at the wave component frequency differences was examined to determine if the controller was required to account for nonlinear loads. Figure 5.15 shows the thruster response amplitude at the frequency difference between wave components for two-component waves at zero and forward speed. The results show that there was some forcing at that frequency differences that the thrusters were required to overcome, and it appears that the nonlinear effects are roughly equivalent to effects at the natural system frequency of 0.4 Hz shown in Figure 5.17.
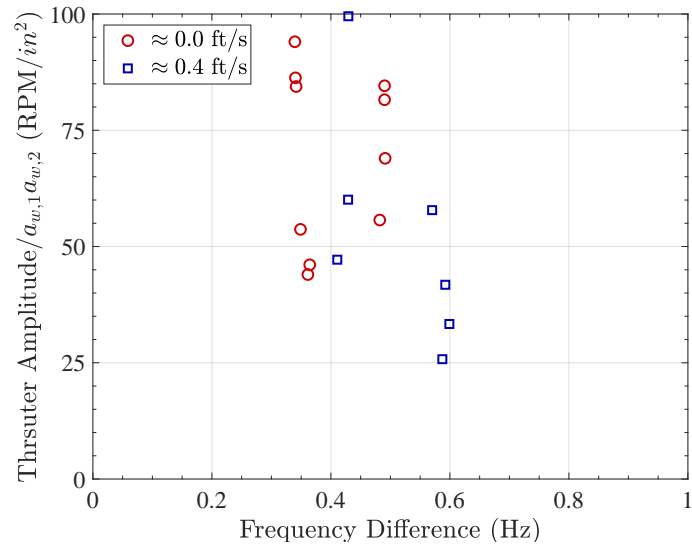
Figure 5.15. Thruster response amplitude as a function of two-component wave frequency difference for zero and forward speeds..

Similar to the pitch and depth responses, the thruster response at the natural system frequencies of 0.1 Hz and 0.4 Hz appears to increase with speed while being independent of wavelength and wave amplitude as shown in Figures 5.16 and 5.17. Additionally, the results showed that the response at 0.1 Hz was also more prominent than the response at 0.4 Hz.

Figure 5.16. Thruster response amplitude at 0.1 Hz system frequency as a function of nondimensional wavelength for various ROV speeds.

Figure 5.17. Thruster response amplitude at 0.4 Hz system frequency as a function of nondimensional wavelength for various ROV speeds.

CHAPTER 6:
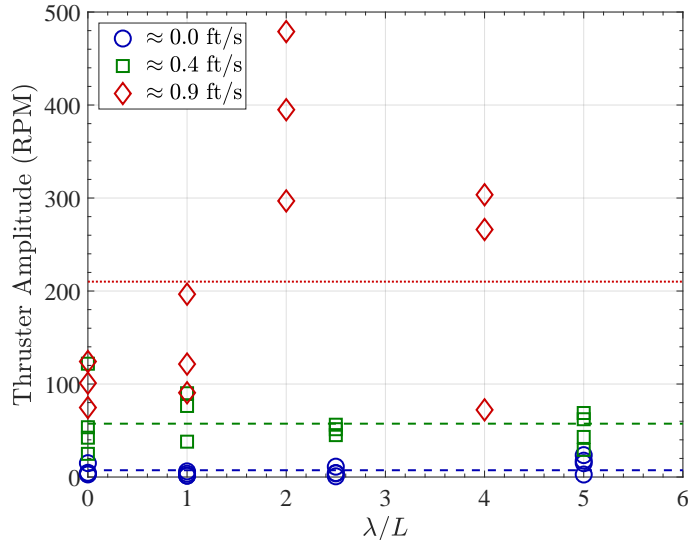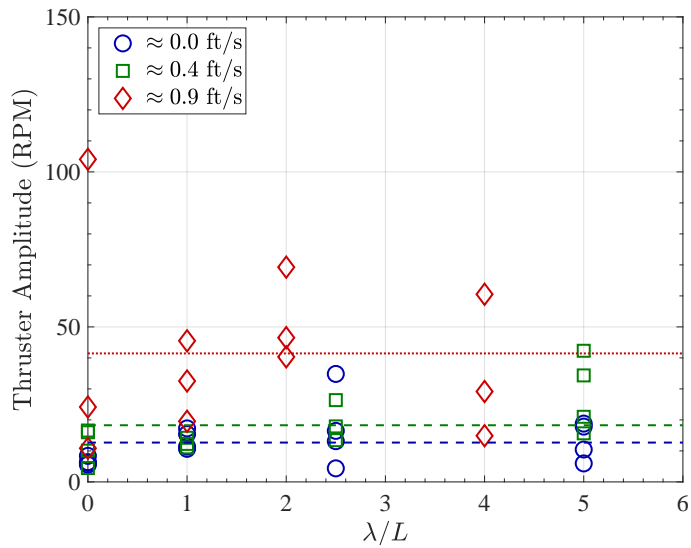# Conclusion and Future Work

6.1 Conclusion

The effects of surface waves on the ROV resulted in unwanted pitch responses stemming from linear loads, nonlinear loads at wave frequency differences for two-component waves, and the natural frequencies of the system. For linear loads, it was shown that the amplitude of the pitch response was dependent on wavelength and scaled linearly with wave amplitude. The response behavior also had a similar, although not identical, dependence on wavelength as the actual linear pitch moment on fixed models used in previous experiments. It was also shown that the pitch response due to linear loads for a single-component wave could be superimposed to generate the response due to linear loads for a two-component wave and potentially for *n* number of wave components. The behavior of the pitch response with respect to frequency differences could not be determined since the frequency difference range examined was small. The pitch response due to the natural system frequencies was shown to be independent of wavelength and wave amplitude but dependent on speed as the response increased with increased speed.

The depth response of the ROV resulting from surface wave effects was minimal due to the ability of the ROV to maintain depth while in the depth hold mode. The ROV had sufficient vertical control authority and response time to minimize the response from wave-induced loads. This can be seen in the thruster response due to linear loads which demonstrated a similar behavior to the pitch response in its dependence on wavelength. For a UUV which lacks sufficient control authority for depth, it is expected that the depth response would follow a similar behavior and dependence on wavelength as pitch did for the ROV. The depth and thruster response at the natural system frequencies also showed a similar behavior to pitch response which was independent of wavelength and wave amplitude but dependent on speed. However, this behavior is only applicable this specific ROV as the frequencies are inherent to the vehicle.

6.2   Future Work

For a given UUV, the response due to surface wave effects is dependent on wave encounter frequency, depth, speed, and relative wave heading. This study accounted for a select number of frequencies, a single wave heading and depth, and had limited control over speed. To better understand the response behavior as a function of wavelength, additional data would need to be collected for an increased number of frequencies, depths, speeds, and wave headings. Doing so would enable the prediction of responses to wave-induced loads and ultimately lead to the development of a dynamic model of the vehicle response which could be used for design optimization as well as improved control systems and autonomous operations.

Further multi-component wave testing could also help determine the response behavior due to nonlinear loads from the frequency difference between underlying component waves. However, it is extremely time consuming to capture these effects experimentally as the response is dependent on the individual components and not only the frequency difference. A better solution would be to determine the response behavior through numerical simulations or empirical models.

Additional experimental studies could also be performed on UUVs of different shapes and sizes and with different control authorities. For example, torpedo-like AUVs, such as the Mk 18 Mod 1 and Mod 2, have a greater length to diameter ratio than the BlueROV2 and also lack vertical thrusters.

List of References

[1] Office of the Chief of Naval Operations. "Autonomous undersea vehicle requirement for 2025," February 18, 2016. [Online]. Available: https://news.usni.org/wp-content/uploads/2016/03/18Feb16-Report-to-Congress-Autonomous-Undersea-Vehicle-Requirement-for-2025.pdf

[2] M. Eckstein. "USNI News Video: Expeditionary minehunting units growing in zize, capabilities," March 4, 2019. [Online]. Available: https://news.usni.org/2019/03/04/usni-news-video-expeditionary-mcm-companies-growing-in-size-capabilities

[3] Department of Defense. "SeaBotix launch," November 7, 2014. [Online]. Available: https://www.defense.gov/observe/photo-gallery/igphoto/2001985118/

[4] W. R. Dean, "On the reflection of surface waves by a submerged circular cylinder," *Mathematical Proceedings of the Cambridge Philosophical Society*, vol. 44, no. 4, pp. 483–491, 1948.

[5] F. Ursell, "Surface waves on deep water in the presence of a submerged circular cylinder. I," *Mathematical Proceedings of the Cambridge Philosophical Society*, vol. 46, no. 1, pp. 141–152, 1950.

[6] F. Ursell, "Surface waves on deep water in the presence of a submerged circular cylinder. II," *Mathematical Proceedings of the Cambridge Philosophical Society*, vol. 46, no. 1, pp. 153–158, 1950.

[7] T. F. Ogilvie, "First- and second-order forces on a cylinder submerged under a free surface," *Journal of Fluid Mechanics*, vol. 16, no. 3, pp. 451–472, 1963.

[8] W. E. Cummins, "Hydrodynamic forces and moments acting on a slender body of revolution moving under a regular train of waves," David Taylor Model Basin, West Bethesda, Maryland, USA, Tech. Rep. 910, December 1954.

[9] P. Wilmott, "On the motion of a slender body submerged beneath surface waves," *Journal of Ship Research*, vol. 32, no. 3, pp. 208–219, 1988.

[10] J. A. Pinkster, "Mean and low frequency wave forces on semi-submersibles," in *Proceedings of the 13th Annual Offshore Technology Conference*, Houston, TX, USA, May 4–7 1981.

[11] T. P. Crook, "An initial assessment of free surface effects on submerged bodies," Master's thesis, Naval Postgraduate School, September 1994.

[12] P. Ananthakrishnan and K. Q. Zhang, "AUV motion in a wave field," in *OCEANS '98 Conference Proceedings*, September 1998, vol. 2, pp. 1059–1063.

[13] M. C. Fang, P. E. Chang, and J. H. Luo, "Wave effects on ascending and descending motions of the autonomous underwater vehicle," *Ocean Engineering*, vol. 33, pp. 1972–1999, 2006.

[14] P. M. Carrica, M. Kerkvliet, F. Quadvlieg, M. Pontarelli, and J. E. Martin, "CFD simulations and experiments of a maneuvering generic submarine and prognosis for simulation of near surface operation," in *Proceedings of the 31st Symposium on Naval Hydrodyanmics*, Monterey, CA, USA, September 2016.

[15] W. E. Cummins, "Forces and moments acting on a submarine moving under waves – comparison of theory with experiments," David Taylor Model Basin, West Bethesda, Maryland, USA, Tech. Rep. C-596, December 1954.

[16] C. J. Henry, M. Martin, and P. Kaplan, "Wave forces on submerged bodies," Davidson Laboratory Stevens Institute of Technology, Hoboken, New Jersey, USA, Tech. Rep. 808, June 1961.

[17] G. M. Khalil, "Experimental investigation of wave forces on submerged horizontal cylinders," *Indian Journal of Engineering and Materials Sciences*, vol. 8, pp. 59–65, 2001.

[18] P. G. Sayer, "Hydrodynamic loads during the deployment of ROVs," *Ocean Engineering*, vol. 35, no. 1, pp. 41–46, 2008.

[19] T. Inoue, H. Suzuki, T. Shimamura, K. Nakajima, and G. Shioji, "Experimental research on horizontal rotation of remotely operated vehicles induced by external forces near the surface of the ocean," *Marine Technology Society Journal*, vol. 43, pp. 5–12, 2009.

[20] L. M. Jones, "Development of a numerical tow tank with wave generation to supplement experimental efforts," M.S. thesis, Dept. Mech. Eng., NPS, Monterey, CA, 2017. [Online]. Available: http://hdl.handle.net/10945/56736

[21] T. M. Turner, J. T. Klamo, and Y. W. Kwon, "Comparison of wave-induced loads on a near surface slender body from inviscid flow linear solution and experimental model test," in *Proceedings of The 37th International Conference on Ocean, Offshore, and Arctic Engineering*, Madrid, Spain, 2018, vol. 7A: Ocean Engineering. [Online]. Available: https://doi.org/10.1115/OMAE2018-77760

[22] T. M. Turner, "Analyzing uuv hull cross-sections for minimizing wave loads when operating near surface," M.S. thesis, Dept. Sys. Eng., NPS, Monterey, CA, 2018. [Online]. Available: http://hdl.handle.net/10945/59606

[23] A. R. Whitmer, "Predicting wave-induced loads in complex seaways on shallowly submerged vessels," M.S. thesis, Dept. Sys. Eng., NPS, Monterey, CA, 2018. [Online]. Available: http://hdl.handle.net/10945/59622

[24] K. Suriben, "Study of wave-induced load effects on a submerged body near the surface," M.S. thesis, Dept. Mech. Eng., NPS, Monterey, CA, 2019. [Online]. Available: http://hdl.handle.net/10945/62748

[25] J. T. Klamo, L. M. Jones, Y. W. Kwon, and J. M. Didoszak, "Upgrades to and current research efforts involving the tow tank facility at the Naval Postgraduate School," in *Proceedings of The 30th American Towing Tank Conference*, 2017.

[26] Blue Robotics. (2020). "BlueROV2," Accessed May 13, 2020. [Online]. Available: https://bluerobotics.com/store/rov/bluerov2/

[27] Blue Robotics. (2020). "BlueROV2 Assembly," Accessed May 13, 2020. [Online]. Available: https://bluerobotics.com/learn/bluerov2-assembly/

[28] Blue Robotics. (2020). "T200 Thruster," Accessed May 13, 2020. [Online]. Available: https://bluerobotics.com/store/thrusters/t200-thruster

THIS PAGE INTENTIONALLY LEFT BLANK

Initial Distribution List

1. Defense Technical Information Center
    Ft. Belvoir, Virginia

2. Dudley Knox Library
    Naval Postgraduate School
    Monterey, California